Speed of dressed-photon–phonon transfer among a small number of particles

M. Ohtsu[1], E. Segawa[2], K. Yuki[3], S. Saito[4] and S. Sangu[5]

[1]Research Origin for Dressed Photon,3-13-19 Moriya-cho, Kanagawa-ku, Yokohama, Kanagawa 221-0022, Japan

[2]Yokohama National University, 79-8 Tokiwadai, Hodogaya-ku, Yokohama, Kanagawa 240-8501, Japan

[3]Middenii, 3-3-13 Nishi-shinjuku, Sinjuku-ku, Tokyo 160-0023, Japan

[4]Kogakuin University, 2665-1, Nakano-machi, Hachioji, Tokyo 192-0015, Japan

[5]Ricoh Co., Ltd., 2-7-1 Izumi, Ebina, Kanagawa 243-0460, Japan

Abstract

This paper analyzes dynamic behaviors of dressed-photon—phonon (DPP) energy transfer by using a blown-up quantum walk model. Numerical calculations are carried out in the case when a large nanometer-sized particle NP_O is surrounded by five small particles NP_Is. Spectral profiles of the DPP transfer indicate that the speeds of the inter-NP transfer, intra-NP transfer, and local transfer are different with each other. This difference is the possible origin of the pulsative behavior found in the transitional period. In the case when the number of the transfer routes is large, the DPP rapidly transfers to reach the NP_O. Conversely, in the case where the number of transfer routes is small, the DPP transfers slowly. It is presumed that such unique nature of the DPP transfer is governed by the off-shell scientific principle of maximizing the average entropy generation.

1 Introduction

Recent theoretical studies have succeeded in drawing a precise physical picture of the creation process of a dressed photon (DP) [1-3]. Furthermore, by using a quantum walk (QW) model, detailed analyses of energy transfers of a dressed-photon−phonon (DPP) among nanometer-sized particles (NPs) have made striking progress. Here, the DPP is a quantum field that is created as a result of interactions between DPs and phonons.

As a successful example of these analyses, the QW model has been used to evaluate the experimental results on optical-wavelength conversion realized by the DPP energy transfer from small NPs to a large NP [4]. Numerical calculations have been carried out in the case where a large NP used as an output signal terminal (OST: NP_O) was surrounded by small NPs used as input signal terminals (ISTs: NP_Is). Figure 1 schematically illustrates this arrangement, in which an NP_O is fixed on a hub [5]. Five NP_Is are fixed on the rim in a rotationally symmetric manner. They are also connected to the NP_O, as represented by spokes. This rim and spoke arrangement represents the DPP energy transfer routes.

Numerical calculations evaluated the stationary values of the input signal transfer rates (ISTR) from the ISTs to the OST. The value of the output signal transfer rate (OSTR) from the OST to the outer space was also evaluated.

Further calculations have been carried out for the case where the rotational symmetry above was broken, that is, when some spokes were lost. The results indicated that the DPP energy transfer routes were a three-fold degenerate bright walk in the case where the number of connected spokes, n_{con}, was odd. Thus, even if some spokes were lost, the stationary values of the OSTR were kept equal to that of n_{con}=5.

In the case where n_{con} was even, the energy transfer routes were composed of bright and dark walks. Since some input signals flowed into the dark walks, the stationary value of the OSTR was smaller than that of the case when n_{con} was odd. The degeneracy in the bright walk and the contribution of the dark walk were found not only in the pentagonal arrangement (Fig. 1) but also in other polygonal arrangements, which demonstrated that their features were independent of the number of NP_Is on the rim.

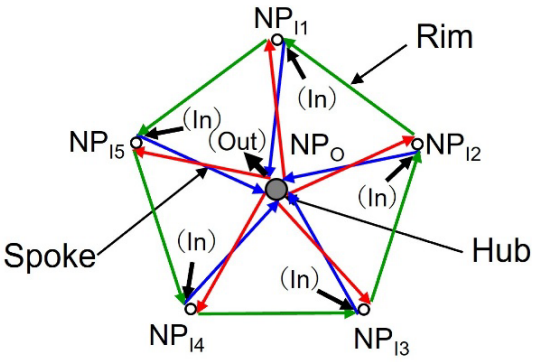

Fig. 1 Arrangement of nanometer-sized particles (NPs).
(In) and (Out) represent an input signal and an output signal, respectively.

It should be noted that the stationary values were governed by the dynamic behavior of the DPP energy transfer in the transitional period prior to reaching the stationary state. A representative feature of such behavior was the pulsative variations of ISTR and OSTR, as shown in Fig.2(a) in ref. [5]. The present paper reports the numerically calculated results of this dynamic behavior.

2 Analyses using a blown-up quantum walk model

The arrangement in Fig. 1 is replaced by Fig. 2 in order to demonstrate a blown-up QW model that was used for analyzing the dynamic behavior [6]. Red arrows represent the inter-NP transfer routes of the DP between adjacent NP_Is and between the NP_Is and NP_O. Small blue circles in the NP_Is and NP_o represent the inner sites that are connected with the red arrows. Blue arrows represent the intra-NP transfer routes of the DP between these inner sites. Green arrows are the self-loops that represent

the local transfer routes of a localized phonon at each inner site. The numbers of the red, blue, and green arrows are 20, 26, and 26, respectively. Thus, the total number of arrows is 72.

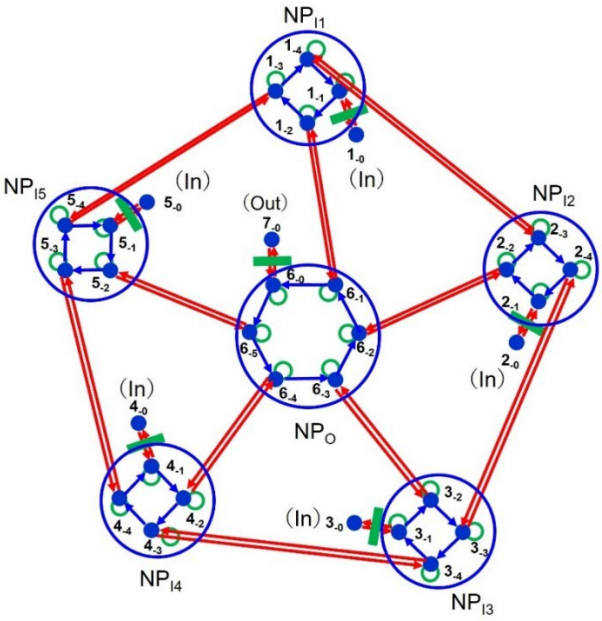

Fig. 2 A blown-up QW model.

A three-row vector is used to represent the probability amplitude of creating the DPP [7]:

$$\vec{\psi}_{t,(x,y)} = \begin{bmatrix} y_{\mathrm{DP+}} \\ y_{\mathrm{DP-}} \\ y_{\mathrm{Phonon}} \end{bmatrix}_{t,(x,y)}, \tag{1}$$

where [ ] represents the vector at time t and at the position (x, y). y_{DP+} and y_{DP-} are the probability amplitudes of the DPs that hop in mutually- opposite directions, and y_{Phonon} is that of the phonon. Its tempo-spatial behavior is derived by solving evolution equations for $\vec{\psi}_{t,(x,y)}$, in which the sum of the coefficient matrices (P_+, P_-, and P_0) is [7]

$$U = \begin{bmatrix} \varepsilon_+ & J & \chi \\ J & \varepsilon_- & \chi \\ \chi & \chi & \varepsilon_0 \end{bmatrix}. \tag{2}$$

Here, off-diagonal elements J and χ are the DP hopping energy and DP-phonon coupling energy, respectively. Diagonal elements $\varepsilon_\pm$ and ε_0 are eigen-energies of DPs and phonon. The numbers of the eigen-vectors and eigen-values of this matrix are both 72, which corresponds to the total number of arrows above. Figure 3 shows the absolute values $|\lambda_n|$ of the eigen-values plotted in descending

order n (=1–72). Their maximum and minimum values are 1.0 and 0.92, respectively.

In order to analyze the features of the DPP transfer rate C_n, the value C_n on each arrow in Fig. 2 is spectrally resolved based on these eigen-values in Fig. 3. Figures 4(a), (b), and (c) show examples of these spectra on red, blue, and green arrows, respectively.

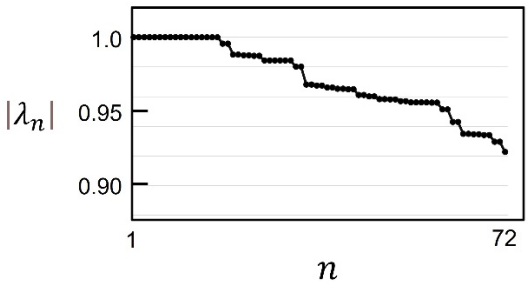

Fig. 3 The absolute values $|\lambda_n|$ of the eigen-values arranged in descending order n (=1–72).

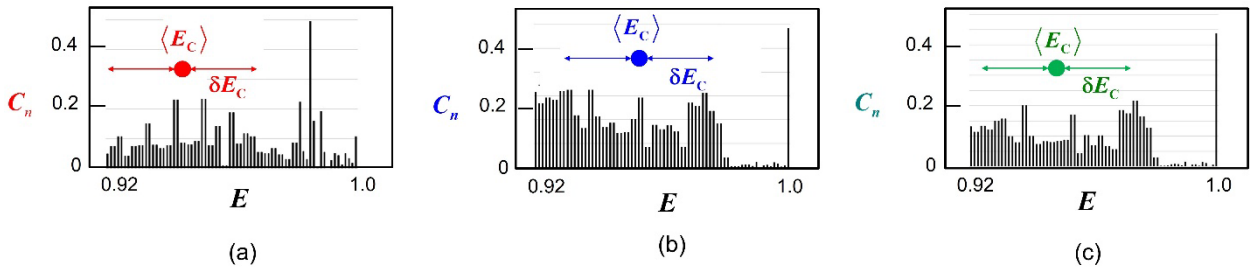

Fig. 4 Examples of spectral profiles.

(a), (b), and (c) are the spectra for the routes of inter-NP transfer ($6_{-1} - 1_{-2}$), intra-NP transfer ($1_{-1} - 1_{-2}$), and local transfer ($1_{-1} - 1_{-1}$), which are represented by the red, blue, and green arrows, respectively.
$\langle E_C \rangle$: The energy at the spectral center. δE_C: The spectral width.

In order to understand the features of these complicated and wide spectral profiles, the energy $\langle E_C \rangle$ at the spectral center is calculated by taking an average of C_n, with $|\lambda_n|$ used as a weighting factor:

$$\langle E_C \rangle = \sum_{n=1}^{72} |\lambda_n| C_n \Big/ \sum_{n=1}^{72} C_n \quad . \tag{3}$$

The spectral width, a measure for representing the magnitude of energy fluctuations, is evaluated by the value of the standard deviation δE_C:

$$\delta E_C = \sqrt{\langle E_C^2 \rangle - \langle E_C \rangle^2} \quad . \tag{4}$$

3 The energy at the spectral center and the magnitude of fluctuations

The left, center, and right parts of Fig. 5 show the energies $\langle E_C \rangle_R$, $\langle E_C \rangle_B$, and $\langle E_C \rangle_G$ at the spectral centers for red (n=1–20), blue (n=21–46), and green (n=47–72) arrows, respectively. This figure indicate that their average values ($\langle \bar{E}_C \rangle_R$, $\langle \bar{E}_C \rangle_B$, and $\langle \bar{E}_C \rangle_G$) satisfy the inequality

$$\langle \bar{E}_C \rangle_G > \langle \bar{E}_C \rangle_R > \langle \bar{E}_C \rangle_B . \tag{5}$$

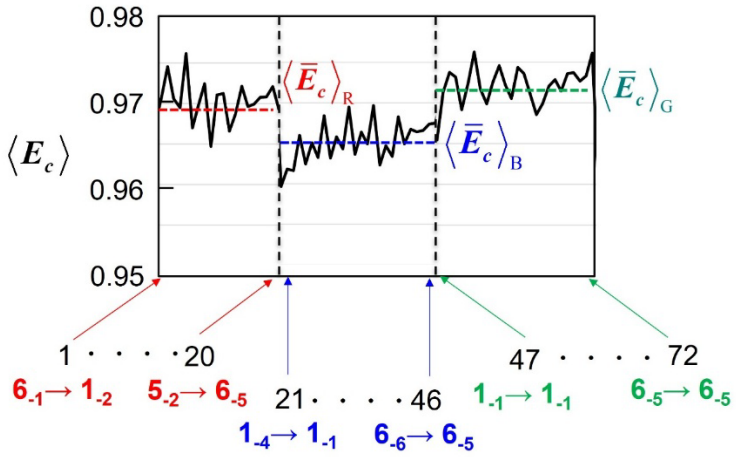

Fig. 5 The energy at the spectral center.
$\langle \bar{E}_C \rangle_R$, $\langle \bar{E}_C \rangle_B$, and $\langle \bar{E}_C \rangle_G$ are the average values for red (n=1–20), blue (n=21–27), and green (n=28–72) arrows. They are represented by horizontal broken lines.

It should be noted that the temporal behavior of the probability amplitude of eq. (1) is the unitary transform of its initial value $\vec{\psi}_{0,(0,0)}$ and is expressed as

$$\vec{\psi}_{t,(x,y)} = \exp(i(E/\hbar)t)\vec{\psi}_{0,(0,0)}, \tag{6}$$

where E is the energy. Since the exponential function in this expression indicates that the speed of the temporal variation of $\vec{\psi}_{t,(x,y)}$ is proportional to E, the inequality of eq. (5) is transformed to

$$s_G > s_R > s_B, \tag{7}$$

where s_R, s_B, and s_G represent the transfer speeds of the DPPs that pass through the red, blue, and green arrows, respectively. That is, the transfer speeds on these arrows are different from each other. This difference is a possible origin of the pulsative behavior that was pointed out at the end of Section 1 (Fig. 2(a) in ref. [5]).

The discussions above are for the arrangement of Figs. 1 and 2, in which five spokes are

connected (n_{con} =5). However, since ref. [5] dealt also with arrangements in which some spokes were lost, the discussions below deal with these arrangements, as shown in Fig. 6. (The arrangement {1} in this figure corresponds to that of Figs. 1 and 2.) Table 1 summarizes the numbers of arrows for arrangements {1} to {9}.

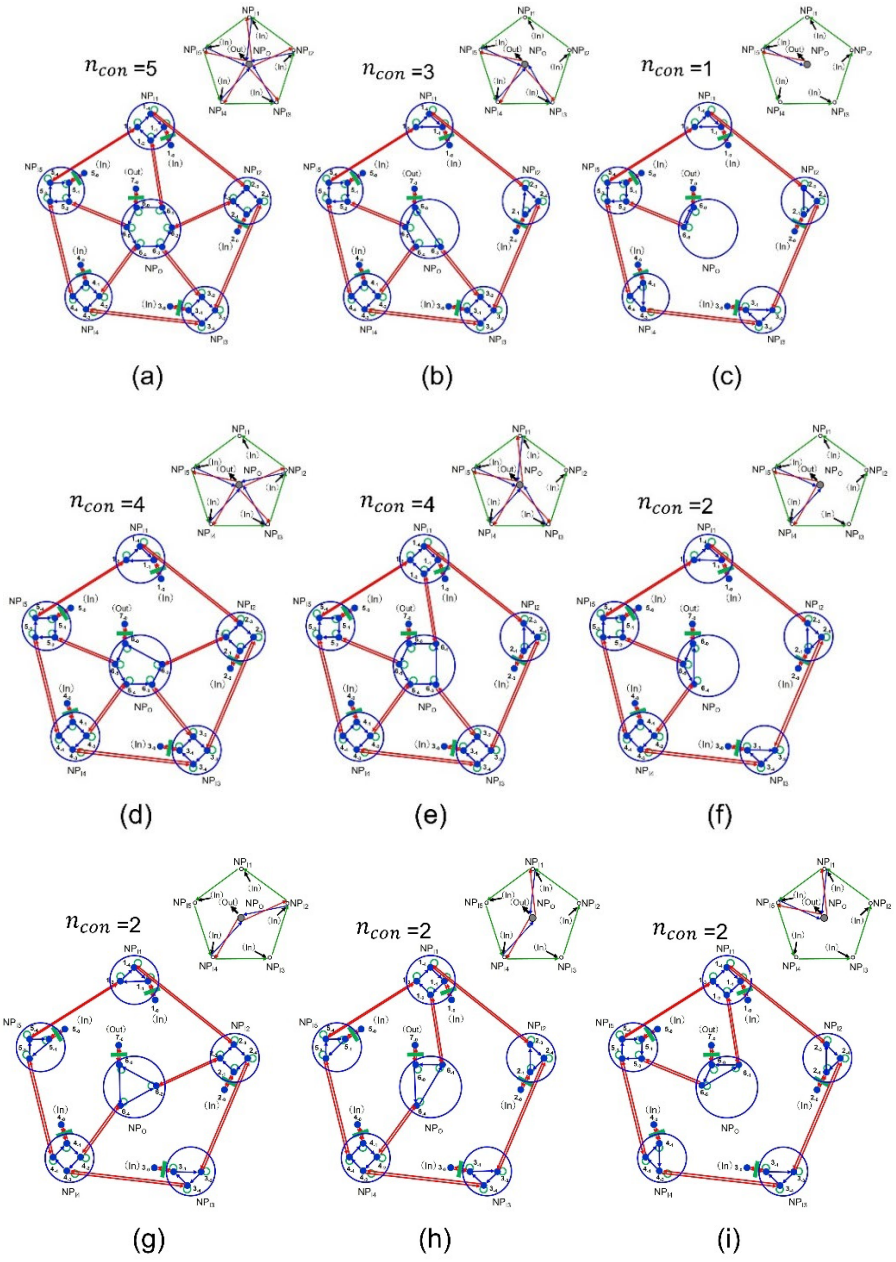

Fig. 6 Blown-up QW models for nine arrangements.

(a)-(c) Arrangements {1}–{3}, for which the number of connected spokes, n_{con}, is odd (=5,3,1).

(d)-(f) Arrangements {4}–{6}, for which the number of connected spokes, n_{con}, is even (=4,4,2).

(g)-(i) Arrangements {7}–{9}, for which the number of connected spokes, n_{con}, is even (=2,2,2).

Table 1 The numbers of arrows for arrangements {1}–{9}.

The number n_{con} of the connected spokes is odd for {1}–{3} and even for {4}–{9}.

Arrangement	n_{con}	Number of red arrows	Number of blue arrows	Number of green arrows	Total number of arrows N
{1}	5	20	26	26	72
{2}	3	16	22	22	60
{3}	1	12	18	18	48
{4}	4	18	24	24	66
{5}	4	18	24	24	66
{6}	2	14	20	20	54
{7}	2	14	20	20	54
{8}	2	14	20	20	54
{9}	2	14	20	20	54

Figure 7(a) shows the averaged values $\langle \bar{E}_{\mathrm{C}} \rangle_{\mathrm{R}}$, $\langle \bar{E}_{\mathrm{C}} \rangle_{\mathrm{B}}$, and $\langle \bar{E}_{\mathrm{C}} \rangle_{\mathrm{G}}$. It shows that the inequality of eq. (5) for arrangement {1} holds also for arrangements {2}–{9}. Furthermore, it shows that the averaged values ($\langle \bar{E}_{\mathrm{C}} \rangle_{\mathrm{R}}$, $\langle \bar{E}_{\mathrm{C}} \rangle_{\mathrm{B}}$, and $\langle \bar{E}_{\mathrm{C}} \rangle_{\mathrm{G}}$) are the smallest for arrangement {3}, in which the n_{con} is the smallest (=1). In contrast, Fig. 7(b) shows that the calculated value of the average $\delta \bar{E}_{\mathrm{C}}$ of the standard deviation of eq. (4) is the largest for arrangement {3} (n_{con}=1).

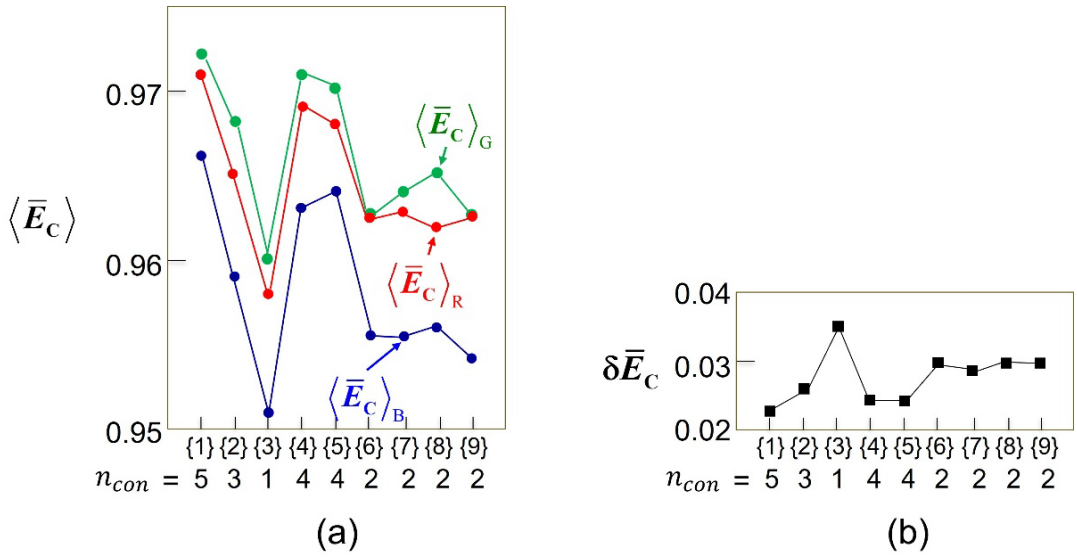

Figures 7 Calculated values for arrangements {1}–{9}.

(a) The value $\langle \bar{E}_{\mathrm{C}} \rangle_{\mathrm{R}}$, $\langle \bar{E}_{\mathrm{C}} \rangle_{\mathrm{B}}$, and $\langle \bar{E}_{\mathrm{C}} \rangle_{\mathrm{G}}$.

(b) The average $\delta \bar{E}_{\mathrm{C}}$ of the standard deviation for the green, red, and blue arrows. Since the values for these three arrows were nearly equal, they are represented by black squares.

4 Relation between the total number of arrows and the transfer speed

Figure 8(a) shows the calculated values of the average $\langle \bar{E}_{\mathrm{C}} \rangle_{\mathrm{Total}}$ that were derived by combining the values of $\langle \bar{E}_{\mathrm{C}} \rangle_{\mathrm{R}}$, $\langle \bar{E}_{\mathrm{C}} \rangle_{\mathrm{B}}$, and $\langle \bar{E}_{\mathrm{C}} \rangle_{\mathrm{G}}$. This figure indicates that the value $\langle \bar{E}_{\mathrm{C}} \rangle_{\mathrm{Total}}$ is the smallest for arrangement {3}, as was the case of Fig. 7(a). It is fairly small for arrangements {6}–{9}.

In order to understand this, Fig. 8(b) shows the values $\langle \bar{E}_{\mathrm{C}} \rangle_{\mathrm{Total}}$ that were plotted as a function of the total number of arrows, N, for arrangements {1}–{9}. By referring to eq. (6), the linear relation between N and $\langle \bar{E}_{\mathrm{C}} \rangle_{\mathrm{Total}}$ in this figure indicates that the transfer speed increases with increasing N. Thus, in the case where the number of connected spokes is large (n_{con}=5; arrangement {1} in Fig.6; N=72), the DPP rapidly transfers to reach the OST even though it has to pass through the large number of arrows. In contrast, in the case of a small n_{con} (n_{con}=1; arrangement {3} in Fig.6; N=48), the DPP slowly transfers to reach the OST even though the number of arrows is small. It can be presumed that such a unique nature of the DPP transfer is governed not by the on-shell scientific principle of least action but by the off-shell scientific principle of maximizing the average entropy generation, as has been pointed out in refs. [8,9].

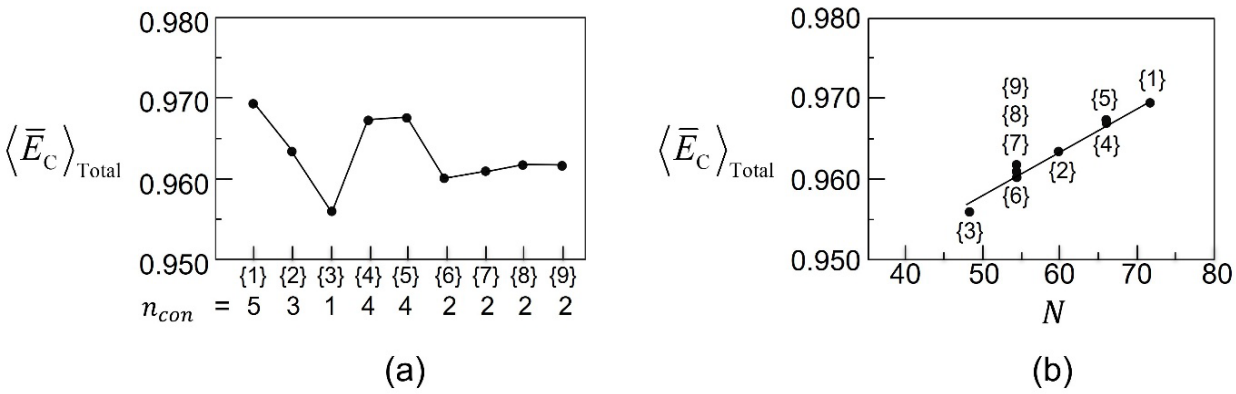

Fig. 8 Calculated values of the average $\langle \bar{E}_{\mathrm{C}} \rangle_{\mathrm{Total}}$.

(a) Horizontal axis: Arrangements {1}–{9} and the number of connected spokes, n_{con}.

(b) Horizontal axis: The total number of arrows, N, for arrangements {1}–{9}.

5 Summary

This paper analyzed the dynamic behavior of DPP energy transfer by using a blown-up quantum walk model. Numerical calculations were carried out in the case where a large $\mathrm{NP_O}$ (an output signal terminal: OST) was surrounded by five small particles $\mathrm{NP_I}$s (input signal terminals: ISTs).

Spectral profiles of the DPP transfer indicated that the speeds of the inter-NP transfer, intra-NP transfer, and local transfer were different from each other. This difference was the possible origin of the pulsative behavior that was found in the transitional period.

In the case where the number of transfer routes was large, the DPP rapidly transferred to reach the OST. In contrast, in the case where this number was small, the DPP transferred slowly. It was presumed that such a unique nature of the DPP transfer is governed by the off-shell scientific principle of maximizing the average entropy generation.

References

[1] H. Sakuma, I. Ojima, M. Ohtsu, and T. Kawazoe, Drastic advancement in nanophotonics achieved by a new dressed photon study," *J. European Opt. Soc.-Rapid Publication* (*JEOS-RP*) (2021) **17**: 28.

[2] H. Sakuma, I. Ojima, and M. Ohtsu, "Perspective on an Emerging Frontier of Nanoscience Opened up by Dressed Photon Studies," *Nanoarchitectonics*, Vol. 5, Issue 1 (2024) pp.1-23.

[3] M. Ohtsu and H. Sakuma, Dressed Photons to Revolutionize Modern Physics (Springer, Heidelberg, 2025).

[4] M. Ohtsu, E. Segawa, K. Yuki, and S. Saito, "Quantum walk analyses of the off-shell scientific features of dressed-photon–phonon transfers among a small number of nanometer-sized particles," *Off-shell Archive* (July, 2024) Offshell: 2407O.001.v1. **DOI** 10.14939/2407O.001.v1

[5]M. Ohtsu, E. Segawa, K. Yuki, and S. Saito, "Bright and dark walks for dressed-photon–phonon transfer," *Off-shell Archive* (January, 2025) Offshell: 2501O.001.v1. **DOI** 10.14939/2501O.001.v1

[6] Y. Higuchi and E. Segawa, "Quantum walks on graphs embedded in orientable surfaces," Annales de l'Institut Henri Poincaré D (2025), Online first, DOI 10.4171/AIHPD/206 arXiv: 2402.00360.

[7] M. Ohtsu, "A Quantum Walk Model for Describing the Energy Transfer of a Dressed Photon," *Off-shell Archive* (September, 2021) Offshell: 2109R.001.v1. **DOI** 10.14939/2109R.001.v1

[8] I. Ojima, "Entropy generation and van Hove limit," Theoretical Particle Physics, vol. 78, no. 2 (1988) pp. B14-B41 (in Japanese). **DOI** https://doi.org/10.24532/soken.78.2_B14

[9] M. Ohtsu, E. Segawa, K. Yuki, and S. Saito, "Optimum dissipation for governing the autonomous transfer of dressed photons, "*Off-shell Archive* (May, 2024) Offshell: 2405O.001.v1. **DOI** 10.14939/2405O.001.v1